Inorganic Chemistry

Article

pubs.acs.org/IC

Metallodithiolates as Ligands to Dinitrosyl Iron Complexes: Toward the Understanding of Structures, Equilibria, and Spin Coupling

Tiffany A. Pinder,[†] Steven K. Montalvo,[†] Chung-Hung Hsieh,[§] Allen M. Lunsford,[†] Ryan D. Bethel,[†] Brad S. Pierce,[‡] and Marcetta Y. Darensbourg*[,†]

[†]Department of Chemistry, Texas A&M University, College Station, Texas 77843, United States

[§]Department of Chemistry, Tamkang University, New Taipei City 25157, Taiwan

[‡]Department of Chemistry and Biochemistry, College of Sciences, The University of Texas at Arlington, Arlington, Texas 76019, United States

Supporting Information

ABSTRACT: Metallodithiolate ligands are used to design heterobimetallic complexes by adduct formation through S-based reactivity. Such adducts of dinitrosyl iron were synthesized with two metalloligands, namely, Ni(bme-daco) and V≡O(bme-daco) (bme-daco = bismercaptoethane diazacyclooctane), and, for comparison, an N-heterocyclic carbene, namely, 1,3-bis(2,4,6-trimethylphenyl)imidazol-2-ylidene (Imes), by cleavage of the $(\mu\text{-I})_2[Fe(NO)_2]_2$ dimer of electronic configuration $\{Fe(NO)_2\}^9$ (Enemark–Feltham notation). With $Fe(NO)_2I$ as Lewis acid acceptor, 1:1 adducts resulted for both the IMes·$Fe(NO)_2I$, complex **2**, and V≡O(bme-daco)·$Fe(NO)_2I$, complex **4**. The NiN_2S_2 demonstrated binding capability at both thiolates, with two $Fe(NO)_2I$ addenda positioned transoid across the NiN_2S_2 square plane, Ni(bme-daco)·$2(Fe(NO)_2I)$, complex **3**. Enhanced binding ability was realized for the dianionic vanadyl dithiolate complex, $[Et_4N]_2[V{\equiv}O(ema)]$, (ema = *N*,*N*′-ethylenebis(2-mercaptoacetamide)), which, unlike the neutral $(V{\equiv}O)N_2S_2$, demonstrated reactivity with the labile tungsten carbonyl complex, *cis*-$W(CO)_4(pip)_2$, (pip = piperidine), yielding $[Et_4N]_2[V{\equiv}O(ema)W(CO)_4]$, complex **1**, whose ν(CO) IR values indicated the dianionic vanadyl metalloligand to be of similar donor ability to the neutral NiN_2S_2 ligands. The solid-state molecular structures of **1**–**4** were determined by X-ray diffraction analyses. Electron paramagnetic resonance (EPR) measurements characterize the $\{Fe(NO)_2\}^9$ complexes in solution, illustrating superhyperfine coupling via the ^{127}I to the unpaired electron on iron for complex **2**. The EPR characterizations of **3** [Ni(bme-daco)·$2(Fe(NO)_2I)$] and **4** [V≡O(bme-daco)·$Fe(NO)_2I$] indicate these complexes are EPR silent, likely due to strong coupling between paramagnetic centers. Within samples of complex **4**, individual paramagnetic centers with localized superhyperfine coupling from the ^{51}V and ^{127}I are observed in a 3:1 ratio, respectively. However, spin quantitation reveals that these species represent a minor fraction (<10%) of the total complex and thus likely represent disassociated paramagnetic sites. Computational studies corroborated the EPR assignments as well as the experimentally observed stability/instability of the heterobimetallic DNIC complexes.

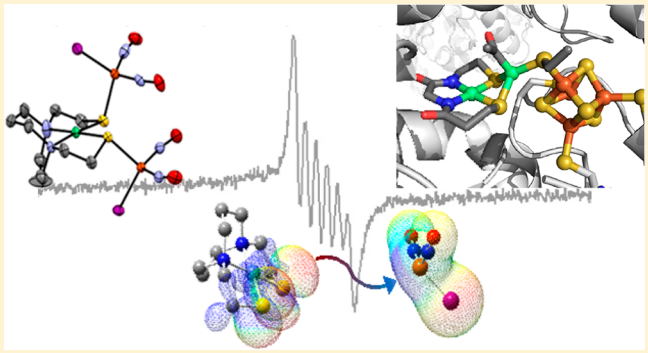

INTRODUCTION

An extensive class of homo- and heterobimetallic complexes has been developed through a bridging thiolate approach, $M{-}(\mu\text{-}SR)_2{-}M'$.[1−3] The active sites of naturally occurring metalloenzymes such as the dinuclear [NiFe]- and [FeFe]-H_2ase further encourage explorations of bridging dithiolates.[4,5] More appropriate to our interest in contiguous N_2S_2 tetradentate ligands is the Ni(Cys-Gly-Cys) tripeptide motif, which serves as a nickel-dithiolate ligand to the catalytically active nickel in the acetyl CoA synthase (ACS) active site, structure **A**, shown in Figure 1.[6]

The distal nickel, Ni_d, in the A-Cluster of acetyl CoA synthase, is in a square planar geometry within the peptidic N_2S_2 binding site. The cis-dithiolates of $NidN_2S_2$ serve as a bidentate S-donor ligand required by the proximal nickel, Ni_p, for facilitation of the C–C and C–S coupling processes in the formation of acetyl CoA.[9,10] It is expected that such contiguous N_2S_2 binding sites could be widespread in bioinorganic chemistry, and thus these binding sites have inspired extensive studies that have characterized other aspects of S-based chemistry, including oxygenation and alkylation.[11,12] In particular, *cis*-dithiolatonickel complexes as metalloligands have not only been used to mimic the structural and redox properties of acetyl CoA synthase, Figure 1B,C,[7,8] but are also

Received: May 13, 2014
Published: August 21, 2014

   dx.doi.org/10.1021/ic501117f | *Inorg. Chem.* 2014, 53, 9095–9105

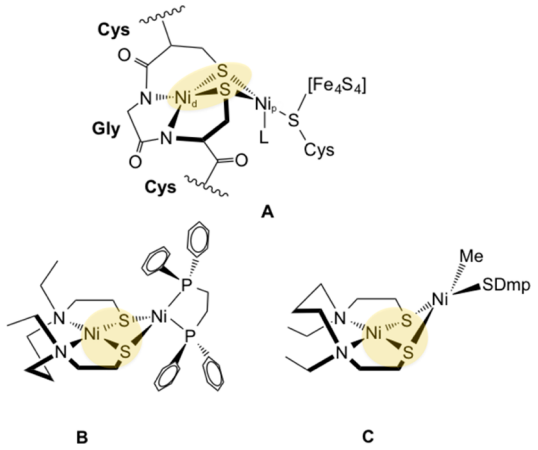

Figure 1. Representation of (A) the A-cluster in acetyl CoA synthase ($Ni_{d,p}$ = distal and proximal to 4Fe4S cluster)[6] and synthetic models (B)[7] and (C),[8] where Dmp = 2,6-di(mesityl)phenyl.[8]

design units for other biomimetics such as [NiFe]-H_2ase active site synthetic analogues.[13−15]

Attempts have been made to codify the electron-donation properties of NiN_2S_2 as metallodithiolate ligands according to ν(CO) stretching frequencies in stable $MN_2S_2{\cdot}W(CO)_{4,5}$ adducts (Chart 1a,b).[16] As stability is a requirement of any analytical standard, the $W(CO)_4$ platform is particularly attractive as a spectroscopic reporter. However, discrimination between the various neutral NiN_2S_2 complexes is minimal, and other reference moieties are of interest. The dinitrosyliron unit, $Fe(NO)_2$, a transition metal acceptor fragment described more fully below, has also been shown to bind to dithiolato−metalloligands; examples are given in Chart 1c,d.[17,18] Complex (**c**), Chart 1, was prepared by Pohl et al., as an analogue to the [NiFe]-H_2ase active site by replacing the $Fe(CO)(CN)_2$ unit with the isoelectronic $Fe(NO)_2$ unit.[17]

The bimetallic molecules represented by Chart 1b include pentacoordinate metallodithiolate ligands in which the fifth donor site of the MN_2S_2 is NO or X^-. In this regard, complexes such as $[Fe(NO)(N_2S_2)]$, $[Co(NO)(N_2S_2)]$, and $[ZnCl(N_2S_2)]^-$ act as bidentate ligands to the tungsten carbonyl synthon.[19,20] Other pentacoordinate N_2S_2 complexes include metal oxo centers such as $[V{\equiv}O]^{2+}$,[21] $[Re{=}O]^{3+}$,[22] and $[Tc{=}O]^{3+}$.[23]

Chart 1. Structures of $MN_2S_2W(CO)_4$ and of NiN_2S_2 as Bi- and Monodentate Ligands to $[Fe(NO)_2]$[10,16−20]

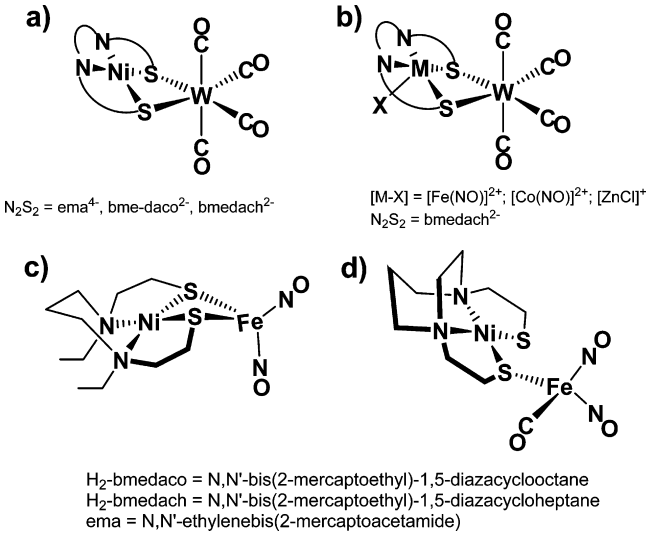

Dinitrosyliron complexes (DNICs) are found in biology and are presumed to play major roles in the storage and transport of NO in cells.[24,25] DNICs exist in two redox levels, which are usually represented via the Enemark−Feltham notation:[26] the oxidized form, $\{Fe(NO)_2\}^9$, has a distinctive electron paramagnetic resonance (EPR) signal at g = 2.03; the reduced form, $\{Fe(NO)_2\}^{10}$, is EPR silent.[27,28] Synthetic models of the physiological DNICs have engaged thiols and imidazoles as mimics of the biologically relevant cysteine and histidine amino acids, respectively.[29,30]

We suggest that the $Fe(NO)_2$ unit can be used, and should be developed, as an additional tool for defining donor properties of metallodithiolates. Not only are the two redox levels stabilized by different ancillary ligands (L) in $L_2Fe(NO)_2$, $[X_2Fe(NO)_2]^-$, and $(L)(X)Fe(NO)_2$ complexes, but within each redox level, the ν(NO) values respond to supporting ligands.[31−33] While most $\{Fe(NO)_2\}^9$ derivatives are in anionic complexes such as $[X_2Fe(NO)_2]^-$, the N-heterocyclic carbene ligand stabilizes a rare example of a neutral species, (IMes)(PhS)$Fe(NO)_2$ (Imes = 1,3-bis(2,4,6-trimethylphenyl)-imidazol-2-ylidene).[34] Without the bulky, strongly bound NHC ligand, the tendency of the $XFe(NO)_2$ moiety to dimerize into very stable $[(\mu\text{-}X)Fe(NO)_2]_2$, well-known in the case of X = SR^- as Roussin's red "esters," prevails.[31,35]

Both NiN_2S_2 and $Fe(NO)N_2S_2$ form S-bridged DNIC adducts, for example, [Ni(bme-dach)·$Fe(NO)_2$CO],[18] [Fe(NO)bme-dach·$Fe(NO)_2]^+$, and [Fe(NO)bme-dach·Fe$(NO)_2$].[34] The rich chemistry and spectroscopic signatures of such derivatives may be expanded by inclusion of the EPR-active vanadyl ion as in $(V{\equiv}O)N_2S_2$ thiolates. Such square pyramidal $(V{\equiv}O)N_2S_2$ complexes have been prepared with dianionic and tetraanionic N_2S_2 ligands and show characteristic EPR signals indicative of the unpaired electron coupling to the ^{51}V metal center of nuclear spin 7/2.[21] While the vanadyl ion substantially deactivates the terminal thiolates, sulfur-based reactivity with electrophiles such as 1,3-dibromopropane and methyl iodide is observed when the overall complex is dianionic $[(V{\equiv}O)N_2S_2]^{2-}$, that is, when N_2S_2 is the tetra-anionic ema ligand, ema = *N*,*N*′-ethylenebis(2-mercaptoacetamide). Herein, we report the reaction and product of a dianionic $[(V{\equiv}O)N_2S_2]^{2-}$ complex with $W(CO)_4$ as a benchmark for comparison to the NiN_2S_2 and $Fe(NO)N_2S_2$ metalloligands. The cleavage products of $(\mu\text{-}I)_2[Fe(NO)_2]_2$ by an N-heterocyclic carbene, and by NiN_2S_2 and $(V{\equiv}O)N_2S_2$ as metalloligands, analyzed according to their structures, spectroscopies, and electrochemistry, are found to inform on the relative qualities of the classical organometallic NHC ligand and the metallodithiolates as ligands.

EXPERIMENTAL SECTION

Methods and Materials. All reactions were carried out with rigorous O_2 exclusion using standard Schlenk techniques or in an argon-filled glovebox. Tetrahydrofuran (THF) and diethyl ether were freshly purified by an MBraun manual solvent purification system packed with Alcoa F200 activated alumina desiccant. The purified THF and diethyl ether were stored with molecular sieves under Ar. The known complexes $Fe(CO)_2(NO)_2$, V≡O(bme-daco), Ni(bme-daco), $[V{\equiv}O(ema)]^{2-}$, ema = *N*,*N*′-ethylenebis(2-mercaptoacetamide), and *cis*-$W(CO)_4(pip)_2$ (pip = piperidine) were prepared according to published procedures.[21,36−39] The IMes NHC ligand

dx.doi.org/10.1021/ic501117f | Inorg. Chem. 2014, 53, 9095−9105

(1,3-bis(2,4,6-trimethylphenyl)imidazol-2-ylidene) was prepared *in situ* by reaction of 1,3-bis(2,4,6-trimethylphenyl)imidazolium chloride with NaOtBu in equivalent stoichiometric amounts. Throughout the manuscript, the IMes NHC ligand will be represented as IMes. The $\{Fe(NO)_2\}^9$ source for complexes **2**, **3**, and **4** was obtained by iodine oxidation of $Fe(CO)_2(NO)_2$, yielding $(\mu\text{-}I)_2[Fe(NO)_2]_2$, isolated as a black, air-sensitive solid, and identified by ν(NO) IR stretching frequencies.[40] The following materials were reagent-grade and used as purchased from Sigma-Aldrich: sodium *tert*-butoxide, 1,3-bis(2,4,6-trimethylphenyl)imidazolium chloride, nitrosonium tetrafluoroborate, and anhydrous dimethylformamide.

Physical Measurements. Infrared spectra were recorded on a Bruker Tensor 37 Fourier transform IR (FTIR) spectrometer. Solution IR spectra were obtained using a CaF_2 cell with a 0.1 mm path length; solid sample IR spectra were obtained using an attenuated total reflectance attachment equipped with a ZnSe crystal. Elemental analyses were performed by Atlantic Microlab, Inc., Norcross, GA. The EPR spectra were collected on a Bruker (Billerica, MA) EMX Plus spectrometer equipped with a bimodal resonator (Bruker model 4116DM). Low-temperature measurements were made using an Oxford ESR900 cryostat and an Oxford ITC 503 temperature controller. EPR spectra parameters were determined by simulations with SpinCount, developed by Prof. M. P. Hendrich of Carnegie Mellon Univ. Single crystals of **2**−**4** were used for Evans' method magnetic susceptibility (d-$CHCl_3$) with values in the range of 1.48−2.01 μ_B.

X-ray Structure Analyses. Low-temperature (110 K) X-ray data were obtained on a single-crystal APEXII CCD diffractometer (Texas A&M University; molybdenum-sealed X-ray tube, Kα = 0.710 73 Å). Space groups were determined on the basis of systematic absences and intensity statistics. Structures were solved by direct methods and refined by full-matrix least-squares on F^2. Hydrogen atoms were placed at idealized positions and refined with fixed isotropic displacement parameters, and anisotropic displacement parameters were employed for all non-hydrogen atoms. The following programs were used: data collection, APEX2;[41] data reductions, *SAINTPLUS*, Version 6.63;[42] absorption correction, *SADABS*;[43] structure solutions, *SHELXS-97* (Sheldrick);[44] and structure refinement, *SHELKL-97* (Sheldrick).[44] Structure plots were generated in Mercury, Version 2.3. Full listings of metric parameters are in the Supporting Information.

Computational Methodology. Geometry optimizations and frequency calculations were performed with the Gaussian 09 suite of programs,[45] utilizing the BP86 functional[46,47] with the 6-311+G(d,p) basis set[48−50] on all atoms, with the exception of iodine, which utilized the Stuttgart/Dresden (SDD) effective core potential (ECP) basis set.[51] The BP86 functional was previously demonstrated to be a suitable combination that best describes the electronic and vibrational structure of dinitrosyl iron complexes.[52] In addition to gas-phase calculations, optimizations were performed with the polarizable continuum model (PCM) of implicit solvation, using THF as the solvent.[53−55] All geometries were fully optimized, starting from the crystal structures where available. Vibrational analyses of all complexes were carried out to obtain the thermodynamic parameters. Each structure was confirmed to be in an energy minimum, with no imaginary frequencies. Free energy corrections to the electronic energy of all complexes were calculated at 298.15 K by Gaussian09;[46] energies were obtained in hartrees and were then converted into kilocalories per mole. Geometric data of the optimized structures were extracted using the Ampac Graphical User Interface (AGUI) program.[56]

Electrochemistry. Cyclic voltammograms (CVs) were recorded on a BAS-100A electrochemical analyzer using a three-electrode cell: a glassy carbon disk (0.071 cm^2), the working electrode; reference electrode, a Vycor-tipped Ag/$AgNO_3$; and a straight platinum wire, the counter electrode. Solutions were deaerated by an Ar purge for 5−10 min, and a blanket of Ar was maintained over the solution while performing the measurements. All experiments were performed at room temperature in CH_2Cl_2 solutions, 2.0 mM in analyte, and containing 0.1 M $(^nBu)_4N^+PF_6^-$ as supporting electrolyte. Ferrocene, Fc, served as the internal reference, and all potentials are reported relative to the Fc/Fc^+ couple as 0.00 V. In the case of complex **2**, full scans in the anodic region saw decomposition of the complex onto the working electrode producing extra events in the cathodic region (Supporting Information, Figure S-5). The working electrode was removed and cleaned, and a CV was obtained of just the cathodic region, which produced a clean voltammogram even upon successive scans (Supporting Information, Figures S-6 and S-7).

Preparation of Compounds. *$[Et_4N]_2[V{\equiv}O(ema)W(CO)_4]$, Complex **1**.* A 0.026 g (0.056 mmol) sample of $(pip)_2W(CO)_4$ was dissolved in 15 mL of dimethylformamide (DMF) and heated at 40 °C for 20 min. The $[Et_4N^+]_2[V{\equiv}O(ema)]^{2-}$ salt (0.029 g, 0.055 mmol), dissolved in DMF, was added dropwise to this solution, and heating was continued for an additional 30 min producing a deep amber color. An air-sensitive, tan-brown solid was obtained from precipitation with diethyl ether. Caramel-colored X-ray quality crystals were grown by diffusion of ether into a DMF solution of the product. Isolation of the crystals afforded 0.021 g (46%) of product. IR (DMF, cm^{-1}) ν(CO) 1996(w), 1919(w), 1872(s), 1848(m), 1802(m). Presumably due to the highly air-sensitive nature of complex **1**, and despite repeated attempts, acceptable elemental analyses were not obtained.

*(IMes)Fe(NO)$_2$I, Complex **2**.* A 0.15 g (0.43 mmol) sample of 1,3-bis(2,4,6-trimethylphenyl)imidazolium chloride and 0.043 g (0.45 mmol) of NaO^tBu were dissolved in 20 mL of THF and stirred for 30 min prior to transfer to a Schlenk flask containing 1.0 mmol of $(\mu\text{-}I)_2[Fe(NO)_2]_2$ dissolved in 10 mL of THF. Stirring for 30 min resulted in a deep greenish-brown solution, which was filtered through Celite. Diethyl ether (10 mL) was added resulting in a dark brown precipitate; the supernatant was removed from the solid via a football cannula. The precipitate was dried in vacuo and redissolved in a minimal amount of THF, transferred to degassed test tubes, and layered with ether to produce X-ray quality crystals. Isolation of the crystals afforded 0.15 g (70%) of product. IR (THF, cm^{-1}) ν(NO) 1782(s), 1726 (vs). Magnetic susceptibility, Evans' method: 1.75 μ_B Anal. Calcd (found) $C_{21}H_{24}FeIN_4O_2$: C, 46.1 (45.9); H, 4.42 (4.48); N, 10.24 (10.00)%.

*[Ni(bme-daco)·(Fe(NO)$_2$I)$_2$] and [V≡O(bme-daco)·Fe(NO)$_2$I], Complexes **3** and **4**.* Complexes **3** and **4** were prepared similarly to **2** by addition of ca. 0.3−0.4 mmol of the metalloligand, Ni(bme-daco) or V≡O(bme-daco) dissolved in 20 mL of THF, to a Schlenk flask containing 1.0 mmol of the $(\mu\text{-}I)_2[Fe(NO)_2]_2$ in 10 mL of THF. Stirring for 30 min resulted in black (the Ni derivative) or deep green (the V≡O derivative) solutions, which were then filtered through Celite. Diethyl ether (10 mL) was added resulting in black ($M = Ni^{2+}$) and deep green (the $[V{\equiv}O]^{2+}$ derivative) precipitates. The supernatant was removed from the solids via a football cannula, and the precipitates were dried and redissolved in THF. The solutions were concentrated in vacuo, transferred to degassed test tubes, and layered with ether to produce X-ray quality crystals. Isolation of the crystals afforded from 0.075 to 0.17 g (45−50%) of product. The IR spectrum of [Ni(bme-daco)·$(Fe(NO)_2I)_2$], (THF, cm^{-1}) ν(NO): 1793(s), 1731 (vs). Anal. Calcd (found) $C_{10}H_{20}Fe_2I_2N_6NiO_4S_2$: C, 15.5 (15.4); H, 2.60 (2.45); N, 10.8 (10.5)%. For [V≡O(bme-daco)·$Fe(NO)_2I$], (THF, cm^{-1}) ν(NO): 1796(s), 1733 (vs). Magnetic susceptibility, Evans' method: variable and in range of 1.4−2.0 μ_B. Anal. Calcd (found) $C_{10}H_{20}FeIN_4O_3S_2V$: C, 22.2 (22.0); H, 3.72 (3.60); N, 10.3 (10.2)%.

RESULTS AND DISCUSSION

Synthesis, Isolation, and Physical Properties. The preparation of a series of MN_2S_2 derivatives of tungsten carbonyls has permitted conclusions regarding their electron donating ability based on ν(CO) frequencies as compared to classical phosphine and amine ligands.[16] Whereas the neutral $(V{\equiv}O)N_2S_2$ complexes displayed no reactivity to *cis*-$(pip)_2W(CO)_4$, the dianionic $[V{\equiv}O(ema)]^{2-}$ displaced the piperidine ligands, yielding complex **1**, eq 1. The yellow-brown crystalline product was isolated as its Et_4N^+ salt by layering an amber DMF solution with Et_2O. Both in solution and as a solid, complex **1** is very air-sensitive. The ν(CO) IR values are close

dx.doi.org/10.1021/ic501117f | Inorg. Chem. 2014, 53, 9095−9105

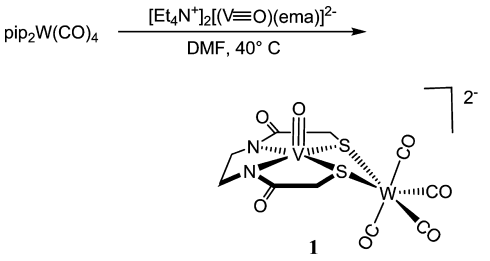

(1)

ν(CO) (DMF, cm-1): 1996, 1872, 1848, 1802

matches of those of the neutral Ni^{II}(bme-daco)·$W(CO)_4$ complex (ν(CO) in DMF (cm^{-1}): 1995, 1871, 1853, 1819).[16] We conclude that the dianionic character of the $[V{\equiv}O(ema)]^{2-}$ metalloligand compensates for the greater electrophilicity of the $[V{\equiv}O]^{2+}$ unit over the d^8 Ni^{II} center.

The reporter $[Fe(NO)_2]^+$ synthon (i.e., the $\{Fe(NO)_2\}^9$ unit) derives from dimeric $(\mu\text{-I})_2[Fe(NO)_2]_2$, first reported by Hieber and Anderson in 1933.[57] Scheme 1 outlines its use in our study. Cleavage of $(\mu\text{-I})_2[Fe(NO)_2]_2$ in THF readily occurred on addition of the *in situ* generated N-heterocyclic carbene, IMes, as well as the NiN_2S_2 and $(V{\equiv}O)N_2S_2$ metalloligands. The (IMes)$Fe(NO)_2$I, **2**, [Ni(bme-daco)·(Fe-$(NO)_2I)_2$], **3**, and [V≡O(bme-daco)·$Fe(NO)_2$I], **4**, complexes were isolated as deep brown, black, and dark green colored crystalline solids, respectively. The $\{Fe(NO)_2\}^9$ complexes are air-sensitive and thermally stable in the solid state, but decompose in solution, even under anaerobic conditions.

Complexes **2** and **3** are highly soluble in THF and CH_2Cl_2, whereas **4** is only moderately soluble. All three complexes (**2**–**4**) were insoluble in toluene; however, toluene/THF mixtures in 3:1 ratio were used for EPR studies, *vide infra*, to repress dissociation. The IR spectra, Figure 2, for **2**–**4** in the diatomic ligand region show two ν(NO) bands of intensity pattern corresponding to the symmetric and asymmetric ν(NO) stretches in the $Fe(NO)_2$ groups. In comparison to the $(\mu\text{-I})_2[Fe(NO)_2]_2$ precursor, of ν(NO) = 1800 and 1736 cm^{-1}, complexes **2**, **3**, and **4** show shifts to lower ν(NO) stretching frequencies, Figure 2.

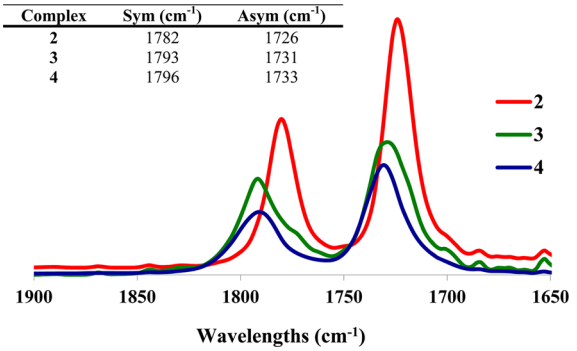

Figure 2. ν(NO) region IR spectra of L(I)$Fe(NO)_2$ complexes, THF solution.

Molecular Structures. The molecular structures of complexes **1**–**4**, characterized by X-ray diffraction analysis, are presented in Figures 3–6. Full structural reports are available in the Supporting Information. Selected bond distances and angles are listed in Table 1 for **2**–**4**.

The tungsten carbonyl adduct of $[Et_4N^+]_2[V{\equiv}O(ema)]^{2-}$, **1**, extends the analogous series of $(NiN_2S_2)W(CO)_4$ complexes.[19,20,58] The $V(\mu\text{-S})_2W$ core has the expected butterfly orientation that yields a V···W distance of 3.30 Å, Figure 3. The vanadyl portion in $[V{\equiv}O(ema)W(CO)_4]^{2-}$ largely maintains the square pyramidal geometry of its precursor, $[V{\equiv}O(ema)]^{2-}$,[21] and the V≡O unit is oriented exo to the W. The V–O bond distance of complex **1** is 1.612(5) Å, and that within the free metalloligand is 1.623(2) Å.[21] While the errors in these values render the distances not significantly different, the apparent shorter V≡O distance correlates with the IR data as the ν(VO) of **1** is ca. 12 cm^{-1} higher than that in the $[Et_4N^+]_2[V{\equiv}O(ema)]^{2-}$. Binding of the $W(CO)_4$ unit to $[V{\equiv}O(ema)]^{2-}$ results in further displacement of the vanadium atom from the N_2S_2 plane, from 0.713 Å in $[V{\equiv}O(ema)]^{2-}$ to 0.729 Å in the V–W bimetallic complex. The N–V–N angle in **1** and its precursor are statistically the same; however, the S–V–S angle in **1** (89.4°) is ca. 4° smaller than it is in $[Et_4N^+]_2[V{\equiv}O(ema)]^{2-}$ (93.9°). This is likely due

Scheme 1. Synthetic Routes to L(I)$Fe(NO)_2$ Complexes[a]

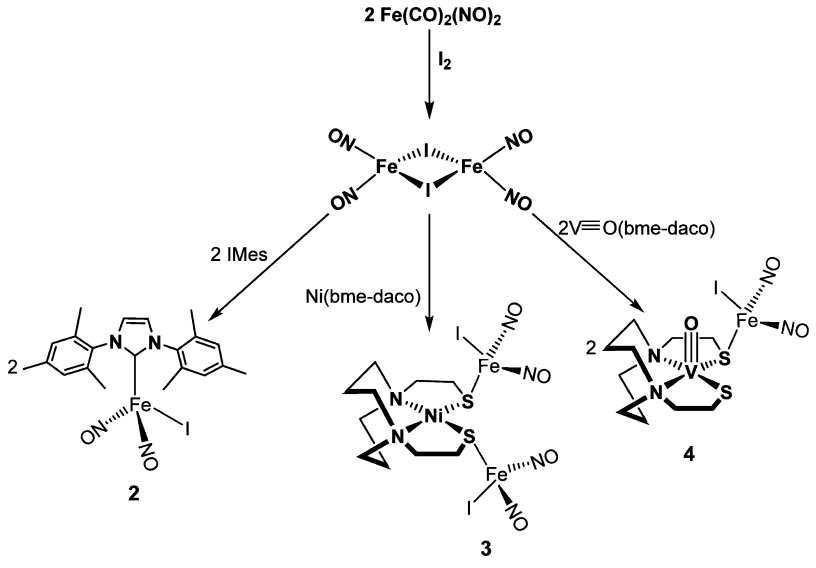

[a]L = NHC or metallodithiolate ligands.

dx.doi.org/10.1021/ic501117f | Inorg. Chem. 2014, 53, 9095–9105

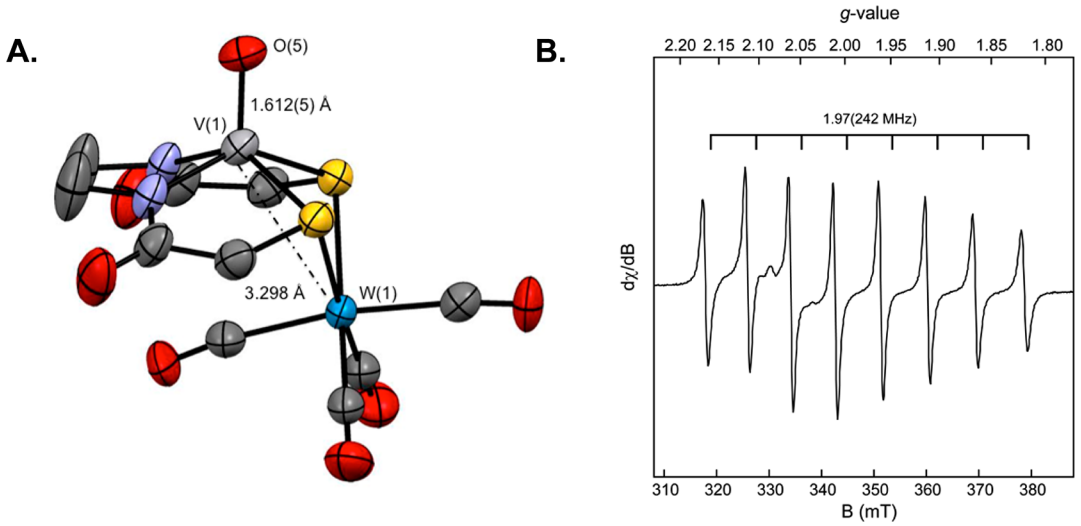

Figure 3. (A) ORTEP drawing of complex **1**, $[Et_4N]_2[V{\equiv}O(ema)W(CO)_4]$, at 50% probability level. Hydrogen atoms and the $[Et_4N]^+$ counterions have been removed for clarity. (B) X-band EPR spectrum of **1** at 298 K in CH_2Cl_2.

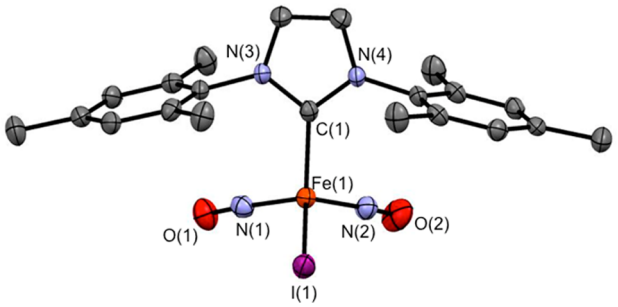

Figure 4. ORTEP drawing of complex **2** with thermal ellipsoids drawn at 50% probability level. Hydrogen atoms have been removed for clarity.

to restriction by the $W(CO)_4$ unit in the bidentate binding mode.

Complexes **2**–**4**, Scheme 1, are based on the $Fe(NO)_2I$ unit as acceptor, with an NHC carbon, **2**, or a metallothiolate sulfur donor, **3** and **4**, in the fourth position of the iron's pseudotetrahedral geometry. In all, the $Fe(NO)_2$ unit is typical of DNICs with slight deviations of the ∠Fe–N–O from linearity that render an inward orientation of the oxygens toward each other. The Fe–N–O angles (Table 1) display slightly greater linearity in **4**, with bond angles of 170.2° and 166.2° (average 168.2°) as compared to **2** and **3**, with average bond angles of 165.0° in **2**, and 164.4° in **3**. Complex **2**, Figure 4, adds to a growing list of DNICs based on and stabilized by N-heterocyclic carbene ligands.[29,34,59−61] The thiolate-bound DNIC $(IMes)Fe(NO)_2SPh$ is a specific analogue to **2**; the difference between the Fe–C_{NHC} distance of these complexes is insignificant.[34] Likewise, the average Fe–NO distances are similar: 1.672(3) Å in the thiolate and 1.689(3) Å in complex **2**.

In complexes **3** and **4** the metallodithiolates are found as monodentate donor ligands to $Fe(NO)_2I$. Complex **3**, of formulation $NiN_2S_2[Fe(NO)_2I]_2$, displays a square planar NiN_2S_2 complex with pendant $Fe(NO)_2I$ units attached to each thiolato-sulfur in a transoid configuration, Figure 5. Metric data for the NiN_2S_2 free ligand is substantially the same as in complex **3** with the exception of a slightly elongated Ni–S distance for **3** versus Ni(bme-daco).[36] Within the $Fe(NO)_2I$ unit, the N–Fe–N is the same as in complex **2**, and the Fe–I distances are identical. Hence, from metric parameters the NiN_2S_2, as a bridging-bidentate metalloligand (i.e., each sulfur donor has been similarly deactivated by the adjacent Lewis acid addendum), has an effect on the $Fe(NO)_2I$ acceptor much like the IMes ligand. It is noteworthy that such a structural motif as found in **3**, in which two S-bound metal acceptors are transoid to an MN_2S_2 plane, has also been observed for a $Cu^{II}N_2S_2$ spanning ligand with two Cu^I pyrazoyl units as acceptors.[37] A similar acceptor also generates a $(Cu^I)_2Ni$ trimetallic via a NiN_2S_2 bridging bidentate ligand.[38]

Although the neutral $(V{\equiv}O)N_2S_2$ complexes have not been observed to form adducts with $W(CO)_4$, the stronger acceptor, $Fe(NO)_2I$, successfully binds V≡O(bme-daco) through a bridging thiolate sulfur similarly to the [Ni(bme-dach)·$Fe(NO)_2(CO)$], a reduced $\{Fe(NO)_2\}^{10}$ DNIC, shown as **D** in Chart 1.[18] Figure 6 displays the structures of complex **4** and the Ni–Fe complex reported in ref 18. Although the vanadyl–oxygen is oriented endo to the $Fe(NO)_2I$ addendum, it does not appear to influence the structure by intramolecular interactions as the shortest distance is that of the $O_{VO}{\cdots}N_{NO}$ bond, which is 3.558 Å. Interestingly, the displacement of $[V{\equiv}O]^{2+}$ from the N_2S_2 plane is maintained the same as in the free $(V{\equiv}O)N_2S_2$ metalloligand, ca. 0.65 Å. The most extreme difference between the two structures in Figure 6 is the pentacoordination feature of $(V{\equiv}O)N_2S_2$, resulting in quite different M–S–Fe angles: 103.7° in **4** and 91.3° in the [Ni(bme-dach)·$Fe(NO)_2(CO)$]. Concomitantly the M–Fe distance increases by ∼0.5 Å in **4**.[18] Despite the difference in redox levels of the $Fe(NO)_2$ moiety in **4** versus [Ni(bme-dach)·$Fe(NO)_2(CO)$], the ∠N–Fe–N value is the same for both, 117°, and some 6° larger than those found in complexes **2** and **3**.

The binding of two $Fe(NO)_2I$ units by Ni(bme-daco) suggests superior electron-donating ability of the nickel versus the vanadyl complexes. In fact all three complexes of this study show ν(NO) IR spectra that are nearly identical in pattern, consistent with the local C_{2v} symmetry of the $Fe(NO)_2$ unit, and in wavenumber position. For comparison, the ν(NO) of the [Ni(bme-dach)·$Fe(NO)_2(CO)$], the reduced$\{Fe(NO)_2\}^{10}$ redox level, are at 1732 and 1689 cm^{-1},[18] which is ∼60 cm^{-1} lower than that of the $\{Fe(NO)_2\}^9$ complexes.

dx.doi.org/10.1021/ic501117f | Inorg. Chem. 2014, 53, 9095−9105

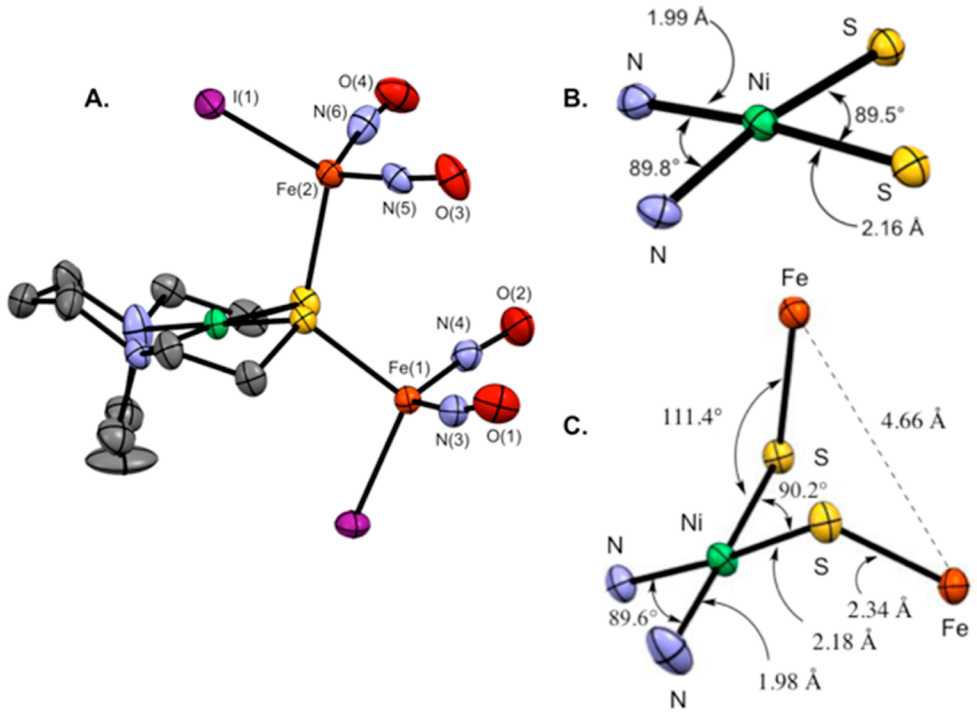

Figure 5. (A) ORTEP rendition of complex **3** with thermal ellipsoids drawn at 50% probability level. (B) Truncated ORTEP drawings of Ni(bme-daco).[36] (C) Complex **3**, comparing local N_2S_2 crystallographic parameters. Hydrogen atoms have been removed for clarity.

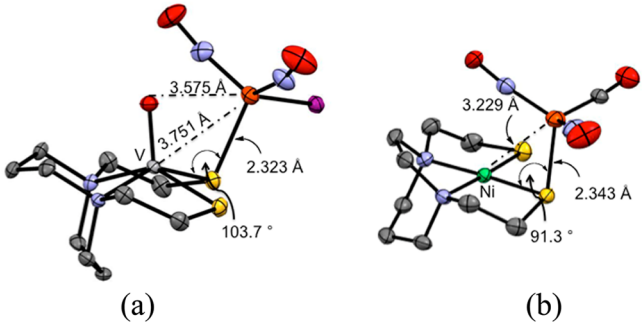

Figure 6. Molecular structures of complex **4** (a) and, for comparison, the [Ni(bme-dach)·Fe(NO)$_2$(CO)], (b),[18] with thermal ellipsoids drawn at 50% probability level. Hydrogen atoms have been removed for clarity.

Table 1. Selected Bond Distances (Å) and Angles (deg) for Complexes 2−4

	2	3	4
Fe−C_{NHC}	2.041(3)		
Fe−S		2.330(1)	2.323(2)
Fe−I	2.574(1)	2.574(1)	2.599(2)
Fe−N_{av}	1.689(3)	1.730(3)	1.688(3)
N−Fe−N	111.9(1)	111.1(2)	117.1(2)
S−Fe−I		109.48(4)	107.01(6)
Fe−N−O	167.3(2)	168.5(3)	170.2(3)
	162.3(3)	161.6(4)	166.2(3)

Electron Paramagnetic Resonance Spectral Data. The paramagnetism due to the {Fe(NO)$_2$}^{9} unit that is latent within the spin-coupled, diamagnetic (μ-I)$_2$[Fe(NO)$_2$]$_2$ may be revealed upon dimer cleavage by exogenous ligands and coordinating solvents. For example, addition of tetraethylammonium iodide ($Et_4N^+I^-$) to (μ-I)$_2$[Fe(NO)$_2$]$_2$ forms the monomeric and paramagnetic [I_2Fe(NO)$_2$]$^-$.[7] Its room-temperature EPR spectrum shows a characteristic isotropic signal centered at g = 2.077 with 11 lines from superhyperfine coupling (hfc) to the two ^{127}I nuclei. These results are consistent with an earlier report of Bryar and Eaton.[7] As our investigation of EPR spectroscopy progressed, the dissociation of the metallodithiolate ligands in THF became apparent; hence, all spectra were subsequently recorded in 3:1 toluene/THF mixtures in which solubility and presumably dissociation were decreased. Complex **2**, a monoiron dinitrosyl complex, {Fe(NO)$_2$}^{9}, has S = 1/2 as determined by magnetic susceptibility, μ = 1.75 μ_B, by both the Evans' and Gouy balance measurements. Its X-band EPR spectrum, Figure 7A, is consistent with an S = 1/2 spin-state with observed g values of $g_{x,y,z}$ = 2.070, 2.068, 2.061. This signal exhibits a six-line pattern centered at g = 2.068 and split by $A_{iso} \approx$ 49 MHz (1.7 mT) resulting from hfc to the single ^{127}I (I = 5/2) nucleus. A quantitative simulation (dashed line) for complex **2** is overlaid on spectrum (A) for comparison. The spectroscopic parameters (g and A values) as well as the concentrations obtained from simulations are provided in Table 2. Nearly 90% (4.4 mM) of the total iron concentration within samples of complex **2** can be attributed to spectrum A. For comparison, the EPR spectrum for an equivalent concentration of complex **3**, [Ni(bme-daco)·(Fe(NO)$_2$I)$_2$], is illustrated in Figure 7B. Although the signal observed for the sample prepared from complex **3** (spectrum B) is similar to that observed for complex **2**, the intensity of spectrum B is nearly 50-fold lower as compared to that of A. Furthermore, while spectrum B exhibits a similar six-line hyperfine splitting from ^{127}I and observable g values, the spectroscopic parameters determined from simulation are easily distinguishable from those obtained for complex **2** [$g_{x,y,z}$ = 2.063, 2.062, 2.054 and $A_{x,y,z}$ = 47, 57, 58 MHz]. Moreover, spin-quantitation of **B** accounts for only ~0.2 mM (4%) of the total iron concentration within the sample. On the basis of this

dx.doi.org/10.1021/ic501117f | Inorg. Chem. 2014, 53, 9095−9105

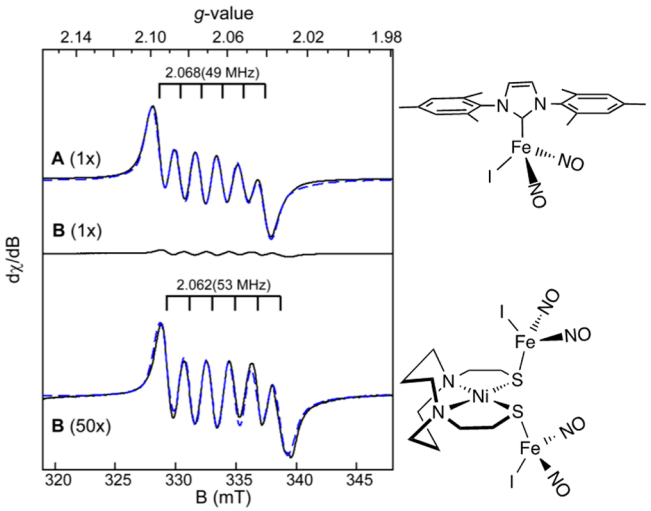

Figure 7. X-band EPR spectra (298 K) of samples prepared from complex **2** (spectrum A) and complex **3** (spectrum B) in 3:1 toluene/THF binary solvent mixture. Spectra are normalized for sample concentration (5 mM), and the observed spin concentration for each species ([**A**] and [**B**]) was determined by quantitative simulation (dashed lines). Instrumental conditions: microwave frequency, 9.64 GHz; microwave power, 63 mW; modulation amplitude, 0.9 mT.

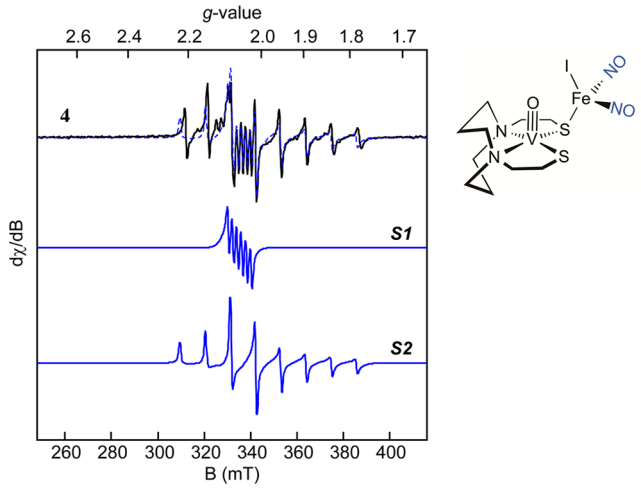

Figure 8. X-band EPR spectrum (298 K) of sample prepared from complex **4** in 3:1 toluene/THF binary solvent mixture. Quantitative simulation (dashed line) is comprised of two spectroscopic contributions (S1) and (S2), see text. Instrumental conditions: microwave frequency, 9.64 GHz; microwave power, 20 mW; modulation amplitude, 0.9 mT. Simulated spin quantitation indicates an S2/S1 ratio of approximately 3:1.

observation, we conclude that the attenuated signal observed within EPR spectrum B represents a minor fraction of solvated (solv)$Fe(NO)_2I$ that disassociated, rather than that of the intact complex **3**.

Assuming strong coupling, complex **3** is expected to exhibit a non-Kramer's integer-spin manifold. If observed, transitions from such doublets are spin-forbidden and thus typically exhibit very weak spectral intensity if observed. For this reason, complex **3** was also characterized at cryogenic temperatures using liquid helium (4−50 K). Furthermore, samples were analyzed using both transverse and parallel microwave field polarizations to maximize the likelihood of observing an integer spin transition. Unfortunately, no additional EPR signals were observed for this sample at liquid helium temperatures. This suggests spin-pairing between the paramagnetic iron centers separated by 4.66 Å resulting in an EPR silent species. Nevertheless, the attenuation of signal intensity of complex **3** relative to **2** suggests ambiguities in structure or equilibria (also influencing variable magnetic susceptibility measurements) that are currently unresolved.

The EPR spectra of [V≡O(bme-daco)·$Fe(NO)_2I$], complex **4**, were obtained at 298 and 10 K. The 298 K spectrum is given in Figure 8 and shows a six-line multiplet superimposed on an eight-line pattern. The former arises from the unpaired electron on the $Fe(NO)_2I$, as seen in Figure 7A,B and is simulated as S1 in Figure 8. Also apparent in this spectrum is the characteristic eight-line EPR hyperfine signature of a vanadyl moeity (^{51}V; I = 7/2), simulated as S2 in Figure 8. At 298 K, the 3:1 simulated mixture of [V≡O] to $Fe(NO)_2I$ paramagnetic species suggests the equilibrium in eq 2 applies. Indeed, cleavage of the (μ-I)$_2$[$Fe(NO)_2$]$_2$ complex can also be observed in both dichloromethane and in THF at room temperature. In these samples, the typical six-line EPR signal associated with the solvated paramagnet (solv)$Fe(NO)_2I$ can readily be observed by EPR in trace quantities. Currently, the origin of this solvent-induced speciation is not entirely clear.

$$3\,[V{\equiv}O(\text{bme-daco})\cdot Fe(NO)_2I] \underset{298\ K}{\rightleftharpoons} 3\,V{\equiv}O(\text{bme-daco}) + (\mu\text{-I})_2[Fe(NO)_2]_2 + (\text{solv})Fe(NO)_2I \quad (2)$$

Computational Studies. Density functional theory (DFT) calculations were designed to further investigate the stability, reactivity, and electronic structure of complexes **2**, **3**, and **4**. As it has been shown to accurately reproduce the electronic environment of the highly delocalized $Fe(NO)_2$ moiety,[52] the BP86 functional[46,47] was selected with the all-electron basis set 6-311+G(d,p)[48−50] on all atoms with the exception of iodine, which utilized the Stuttgart/Dresden (SDD) effective core potential (ECP) basis set.[51] To aid in interpretation of the EPR spectra, the atomic spin densities of complexes **2**, **3**, and **4** were analyzed from single-point calculations that utilized the same 6-

Table 2. Comparison of Experimental EPR Parameters of Complexes 2, 3, and 4 from 298 K Spectra

		effective S = 1/2 representation						
complex	EPR-active nuclei	g_x	g_y	g_z	A_x (MHz)	A_y (MHz)	A_z (MHz)	theoretical[a] concentration (mM)
2	^{127}I (I = 5/2)	2.070	2.068	2.061	43	52	56	4.4
3	^{127}I (I = 5/2)	2.063	2.062	2.054	47	57	58	0.2
4	^{127}I (I = 5/2)	2.074	2.054	2.049	47	58	37	
4	^{51}V (I = 7/2)	1.966	1.982	2.040	315	283		

[a]Experimental concentrations from 5 mM solutions.

dx.doi.org/10.1021/ic501117f | Inorg. Chem. 2014, 53, 9095−9105

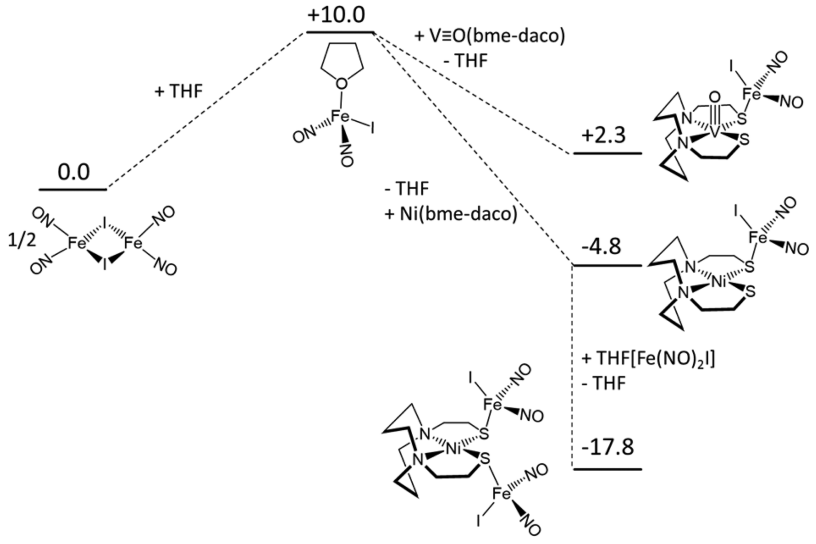

Figure 9. Calculated gas-phase relative stabilities of $\{Fe(NO)_2\}^9$ complexes $[N_2S_2(V{\equiv}O)[Fe(NO)_2I]$, $[N_2S_2(Ni)[Fe(NO)_2I]$, and $[N_2S_2(V{\equiv}O)[Fe(NO)_2I]_2$ versus the $[(\mu\text{-}I)Fe(NO)_2]_2$ dimer by way of a putative THF adduct $(THF)[Fe(NO)_2I]$.

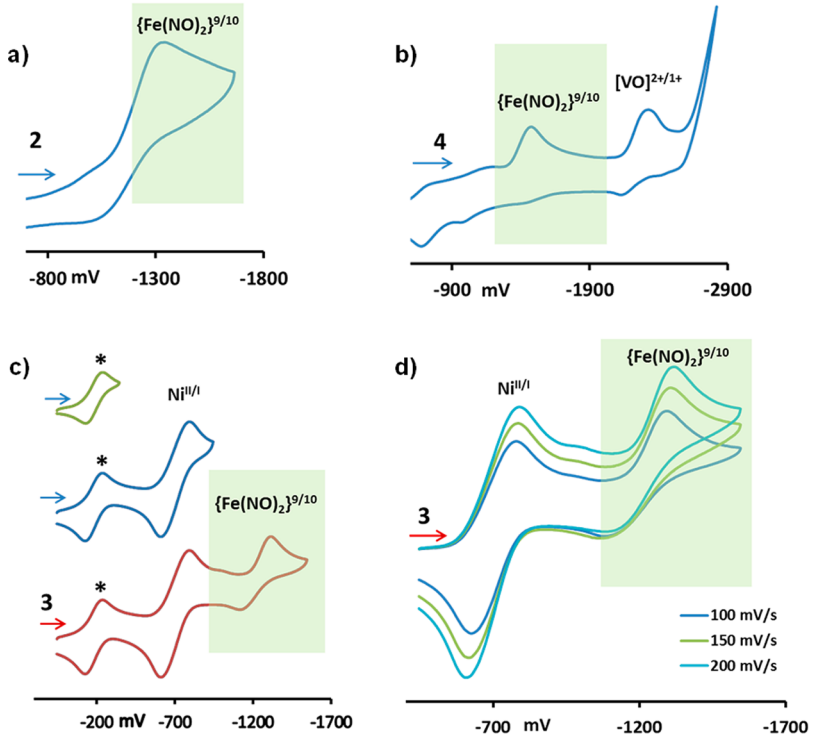

Figure 10. Cyclic voltammograms, 200 mV/s, of 2 mM CH_2Cl_2 solutions (referenced to Fc/Fc^+ = 0.0 mV) of complex **2** (a), complex **4** (b), and complex **3** (c), with assignments to the metals within the metallodithiolate ligands and the $\{Fe(NO)_2\}^{9/10}$ couple in each. The fully reproducible starred feature in (c) is not assigned. CVs of complex **3** under variable scan rates are shown in (d).

311G(d,p) basis set without the inclusion of the diffusion term. All three complexes were found to have slightly more than one (~1.2) unpaired electron per iron atom, with ~0.2 unpaired electrons on each iodine atom. The nitrogen and oxygen atoms of the NO ligands had ~0.25 unpaired electrons as a unit. For complex **4**, the unpaired electron, of spin α, residing primarily on the vanadium, spin polarizes the electron distribution of energetically similar orbitals due to the different interactions with the α and β electrons in those orbitals. This spin contamination of the frontier molecular orbitals is reduced by the use of a pure DFT functional, but even BP86 has been shown to overestimate spin polarization.[63] Therefore, the excess β spin density on the NO ligands is seen only in the computational results and is not observed experimentally (i.e., by EPR). This lack of nitrogen hyperfine coupling is present in many $\{Fe(NO)_2\}^9$ complexes, including the (IMes)Fe-$(NO)_2$SPh analog of **2**, calculations of which show similar β spin density on the NO ligands.[61] The only other instance of unpaired α spin density is seen with complex **4**, in which the vanadyl moiety has ~1 unpaired electron.

As the stability of the MN_2S_2–DNIC adducts was uncertain in a coordinating THF solution, the possibility of solvent

dx.doi.org/10.1021/ic501117f | Inorg. Chem. 2014, 53, 9095−9105

displacement of the metalloligand, forming either the THF−DNIC adduct or the $[(\mu\text{-I})Fe(NO)_2]_2$ dimer, was investigated. Therefore, the relative free energy of the possible products formed in the reaction of $[(\mu\text{-I})Fe(NO)_2]_2$ with free metalloligands $(V{\equiv}O)N_2S_2$ and NiN_2S_2 in THF solvent were compared, Figure 9. Addition of THF to $[(\mu\text{-I})Fe(NO)_2]_2$ yields the THF-adduct $(C_4H_8O)[Fe(NO)_2I]$, a paramagnetic $\{Fe(NO)_2\}^9$ species, which is calculated to be less stable than the dimer (plus THF) by 10.0 kcal/mol. The gas-phase addition of the $(V{\equiv}O)N_2S_2$ metalloligand to 1/2 $[(\mu\text{-I})Fe(NO)_2]_2$ yields complex **4**, which is calculated to be 2.3 kcal/mol less stable than the free vanadyl complex and the iron dinitrosyl dimer. In calculations utilizing a THF solvent continuum, the dimer is destabilized, resulting in a 3.2 kcal/mol stabilization of **4** versus the free vanadyl and $[(\mu\text{-I})Fe(NO)_2]_2$.

The product of the addition of a single $[Fe(NO)_2I]$ moiety to the NiN_2S_2 metalloligand generates a paramagnetic $\{Fe(NO)_2\}^9$ complex, **3a**, that is some 4.8 kcal/mol more stable than the free metalloligand and the $[(\mu\text{-I})Fe(NO)_2]_2$ starting materials. A second $[Fe(NO)_2I]$ moiety can then be added to this complex, yielding a stable triplet structure, **3**. Complex **3** is 17.8 kcal/mol more stable than the free metalloligand and $[(\mu\text{-I})Fe(NO)_2]_2$. The $Fe(NO)_2I$ spin-paired singlet species was optimized independently and was found to be less stable than the triplet by 13.0 kcal/mol.

The calculated relative stabilities of the $[Fe(NO)_2I]$ moiety as a dimer versus metallodithiolate-bound supports the conclusions from EPR spectral data, *vide supra*. The computational (gas phase) stabilities suggest $Ni(N_2S_2)[Fe(NO)_2I]_2$ remains intact, but the $[(V{\equiv}O)N_2S_2[Fe(NO)_2I]$ may break apart into $(V{\equiv}O)N_2S_2$ and $[(\mu\text{-I})Fe(NO)_2]_2$ components. A low-energy intermediate along this reaction pathway, the solvent adduct $(THF)[Fe(NO)_2I]$ is a possible source of the EPR signal observed in THF solutions of the $[Fe(NO)_2I]_2$ dimer at 298 K.

Electrochemistry. CVs of dinitrosyl iron complexes are dominated by the $\{Fe(NO)_2\}^{9/10}$ couple, the value of which strongly depends on the L or X^- ligands within the coordination sphere of Fe. Thus, the single irreversible reduction event at −1.33 V for complex **2**, the NHC derivative of $Fe(NO)_2I$, Figure 10a, is assigned with confidence to the $\{Fe(NO)_2\}^{9/10}$ couple, consistent with earlier results found for the analogous $(NHC)Fe(NO)_2SPh$ complex, −1.48 V.[34] Complexes **3** and **4** show similar events at −1.37 and −1.47 V, respectively, which are also assigned to the $\{Fe(NO)_2\}^{9/10}$ couple, Figure 10. The other reduction features in these two complexes are due to the metal within the N_2S_2 binding site.

The $Ni^{II/I}$ couple in NiN_2S_2 complexes has a clear response to S-modification by electrophiles, shifting positively by 700 mV in the cationic complex resulting from a single S-methylation and by another 500 mV in the dimethylated dication, Table 3.[11] Likewise in the trimetallic nickel dicationic complex, in which a single nickel ion links two Ni(bme-daco) units, the $Ni^{II/I}$ couple within the NiN_2S_2 metalloligands is some 1.2 V more accessible than it is in the free, neutral NiN_2S_2. In complex **3**, the quasi-reversible couple centered at −0.70 V with an i_{pa}/i_{pc} of 0.79 is reasonably assigned to the Ni^{II}/Ni^{I} couple. It is positively shifted from the parent Ni(bme-daco) complex by 1.64 V, consistent with the double metalation by $Fe(NO)_2I$ units. In contrast to the CV of complex **3**, the prominent additional reductive event observed in that of complex **4** (in CH_2Cl_2 solvent) is at −2.35 V which is largely

Table 3. Listing of Cyclic Voltammetry Parameters

entry[a]	E_{pc} $Fe(NO)_2^{9/10}$ [V]	$E_{1/2}$ M[b] [V]
2	−1.33	
3	−1.37	−0.70
4	−1.47	(−2.35)
VO(bme-daco)		−2.50
Ni(bme-daco)		−2.34[11]
$Ni(bme\text{-}daco)Me^+$		−1.60[11]
$Ni(bme\text{-}daco)Me_2^{2+}$		−1.08[11]
$[Ni(bme\text{-}daco)]_2Ni^{2+}$		−1.11[11]

[a]All measurements were carried out in CH_2Cl_2 solution (with exception of VO(bme-daco), which was done in DMF), 0.1 M $(^nBu)_4N^+PF_6^-$ electrolyte, measured vs $Ag/AgNO_3$ reference electrode, with a concentration from 1.0 to 2.5 mM in analyte. All potentials are referenced to Cp_2Fe/Cp_2Fe^+ = 0 mV as internal standard. [b]M denotes either the $Ni^{2+/1+}$ redox couple in the case of complex **3** and the S-alkylated or S-metalated Ni(bme-daco) compounds as references or the $[VO]^{2+/1+}$ redox couple in the case of complex **4** and VO(bme-daco). See text for discussion.

the same as for the free V≡O(bme-daco) complex, −2.50 V (in DMF solvent). This result suggests either a very poor interaction of the $Fe(NO)_2I$ unit with the sulfurs, or, indeed, the dissociation equilibria, eq 2, lies to the right under the electrochemical conditions. Alternatively, the $Fe(NO)_2I$ unit could exist as a solvate; either possibility releases the V≡O(bme-daco), resulting in the highly negative redox event.

Such a conclusion regarding the dissociation of the $[V{\equiv}O(bme\text{-}daco){\cdot}Fe(NO)_2I]$ adduct is consistent with the computational studies above. Furthermore, attempts to correlate ν(NO) IR stretching frequencies with the $\{Fe(NO)_2\}^{9/10}$ reduction events were not satisfactory if the assumption is made that the complex **4** remains intact under the conditions of the electrochemical studies. That is, the ν(NO) IR data suggest the electron density within $Fe(NO)_2$ unit to be in the order of **4** < **3** < **2**, while the electrochemical data suggests the reduction potentials ascribed to the $Fe(NO)_2$ unit are in the opposite order. That is, the least electron-rich (by IR data) complex **4** should be the most easily reduced; instead, it has the *least* accessible reduction. We evade this conundrum by accepting that the solution dielectric within the electrochemical experiments substantially modifies the components that we seek to correlate.

The $\{Fe(NO)_2\}^9$ complexes of this study, **2**−**4**, exhibit irreversible oxidation events between 0.20 and 0.60 V. Full electrochemical scans as well as various scan rates can be found in the Supporting Information.

■ CONCLUSIONS

The use of $W(CO)_4$ and $Fe(NO)_2$ as acceptors and reporter units for the donor abilities of metallodithiolate ligands, as benchmarked by an N-heterocyclic carbene ligand,[62] has been explored. Our study finds consistencies in matches of acceptor with metallo−dithiolate donors, which permits a wider application of such synthetic approaches to heterobimetallic complexes.[64] For example, the Ni(bme-daco), which readily binds to $W(CO)_4$ as a bidentate ligand, also serves as a bridging bidentate ligand to $\{Fe(NO)_2\}^9$, utilizing both *cis*-dithiolate sulfurs in monodentate binding to two $Fe(NO)_2I$ units. In contrast a single NiN_2S_2 binds to $Fe(NO)_2(CO)$ in which the dinitrosyl iron unit is in its reduced redox level, $\{Fe(NO)_2\}^{10}$, leaving an unbound thiolate on Ni^{II}. The analogous neutral metalloligand, V≡O(bme-daco), has such sulfur deactivation

dx.doi.org/10.1021/ic501117f | Inorg. Chem. 2014, 53, 9095−9105

that the $W(CO)_4$ adduct cannot be formed; however, with the stronger $Fe(NO)_2I$ acceptor, the isolation of [V≡O(bme-daco)·$Fe(NO)_2I$] provides an alternate exemplar to previous studies that indicated no reactivity of the *cis*-thiolates of neutral $(V{\equiv}O)N_2S_2$ complexes with alkylating agents as electrophiles.

The donor ability of the ligands used in this study can be ranked based on the ν(NO) IR stretching frequencies of the $Fe(NO)_2$ unit, in the order (IMes) > Ni(bme-daco) > V≡O(bme-daco). The computations corroborate the deactivation of the sulfur donors by the vanadyl ion in comparison to the Ni^{2+}, confirming the poor donor ability and the likelihood of dissociation of the [V≡O(bme-daco)·$Fe(NO)_2I$] adduct in solution, as found in the EPR and electrochemical studies.

EPR spectroscopy showed superhyperfine coupling between various connected EPR active centers in the case of ^{127}I with the unpaired electron on the iron center of the $\{Fe(NO)_2\}^9$ unit of **2** and the solvated (solv)$Fe(NO)_2I$ centers disassociated from **3** and **4**. Given the absence of an observable EPR signal associated with the intact complex **3**, it can be inferred that the two $\{Fe(NO)_2\}^9$ centers (with Fe···Fe distance 4.66 Å) are spin-coupled through the NiN_2S_2 spanning ligand. Similarly, in complex **4**, the paramagnetic ^{51}V metal ion in vanadyl and the ^{127}I in the $Fe(NO)_2I$ unit (at a V···Fe distance of 3.75 Å) also appear to be strongly coupled. However, the disassociated paramagnetic centers, observed in a 3:1 ratio, contribute to two distinct superhyperfine patterns with no overlap. Computational results help explain the experimental evidence; however, direct measurements of the equilibria are not available at this time. Overall, the complexes reported emphasize the stability of the intact $Fe(NO)_2$ unit and stress its spectroscopic and redox properties, which are sensitive reporters of its addenda. The new complexes expand the growing list of examples of MN_2S_2 complexes as mono- and bidentate *cis*-dithiolato−metalloligands, thereby serving as mutual informants on the acceptor properties of the units to which they bind.

■ ASSOCIATED CONTENT

Ⓢ Supporting Information

X-ray crystallographic data (CIF) from the structure determinations, ORTEPs, full lists of metric parameters for complexes **1**−**4**, EPR data, and additional electrochemical scans (complexes **2**−**4**). This material is available free of charge via the Internet at http://pubs.acs.org.

■ AUTHOR INFORMATION

Corresponding Author

*E-mail: marcetta@chem.tamu.edu.

Notes

The authors declare no competing financial interest.

■ ACKNOWLEDGMENTS

We are grateful for financial support from the National Science Foundation (CHE-0910679 and CHE-1266097 to M.Y.D.; and CHE-1213655 to B.S.P.) and the Robert A. Welch Foundation (A-0924 to M.Y.D.).

■ REFERENCES

(1) Zhu, W.; Marr, A. C.; Wang, Q.; Neese, F.; Spencer, D. J. E.; Blake, A. J.; Cooke, P. A.; Wilson, C.; Schröder, M. *Proc. Natl. Acad. Sci. U.S.A.* **2005**, *102*, 18280−18285.

(2) Verhagen, J. A. W.; Lutz, M.; Spek, A. L.; Bouwman, E. *Eur. J. Inorg. Chem.* **2003**, *2003*, 3968−3974.

(3) Liaw, W.-F.; Chiang, C.-Y.; Lee, G.-H.; Peng, S.-M.; Lai, C.-H.; Darensbourg, M. Y. *Inorg. Chem.* **2000**, *39*, 480−484.

(4) Volbeda, A.; Charon, M.-H.; Piras, C.; Hatchikian, E. C.; Frey, M.; Fontecilla-Camps, J. C. *Nature* **1995**, *373*, 580−587.

(5) Peters, J. W.; Lanzilotta, W. N.; Lemon, B. J.; Seefeldt, L. C. *Science* **1998**, *282*, 1853−1858.

(6) Darnault, C.; Volbeda, A.; Kim, E. J.; Legrand, P.; Vernede, X.; Lindahl, P. A.; Fontecilla-Camps, J. C. *Nat. Struct. Biol.* **2003**, *10*, 271.

(7) Wang, Q.; Blake, A. J.; Davies, E. S.; McInnes, E. J. L.; Wilson, C.; Schröder, M. *Chem. Commun. (Cambridge, U.K.)* **2003**, 3012−3013.

(8) Ito, M.; Kotera, M.; Matsumoto, T.; Tatsumi, K. *Proc. Nat. Acad. Sci. U.S.A.* **2009**, *106*, 11862−11866.

(9) Webster, C. E.; Darensbourg, M. Y.; Lindahl, P. A.; Hall, M. B. *J. Am. Chem. Soc.* **2004**, *126*, 3410−3411.

(10) Amara, P.; Volbeda, A.; Fontecilla-Camps, J. C.; Field, M. J. *J. Am. Chem. Soc.* **2005**, *127*, 2776−2784.

(11) Farmer, P. J.; Solouki, T.; Mills, D. K.; Soma, T.; Russell, D. H.; Reibenspies, J. H.; Darensbourg, M. Y. *J. Am. Chem. Soc.* **1992**, *114*, 4601−4605.

(12) Grapperhaus, C. A.; Darensbourg, M. Y. *Acc. Chem. Res.* **1998**, *31*, 451−459.

(13) Ogo, S.; Kabe, R.; Uehara, K.; Kure, B.; Nishimura, T.; Menon, S. C.; Harada, R.; Fukuzumi, S.; Higuchi, Y.; Ohhara, T.; Tamada, T.; Kuroki, R. *Science* **2007**, *316*, 585−587.

(14) Reynolds, M. A.; Rauchfuss, T. B.; Wilson, S. R. *Organometallics* **2003**, *22*, 1619−1625.

(15) Ohiki, Y.; Tatsumi, K. *Eur. J. Inorg. Chem.* **2011**, 973−985.

(16) Rampersad, M. V.; Jeffery, S. P.; Golden, M. L.; Lee, J.; Reibenspies, J. H.; Darensbourg, D. J.; Darensbourg, M. Y. *J. Am. Chem. Soc.* **2005**, *127*, 17323−17334.

(17) Osterloh, F.; Saak, W.; Haase, D.; Pohl, S. *Chem. Commun. (Cambridge, U.K.)* **1997**, *0*, 979−980.

(18) Hsieh, C.-H.; Chupik, R. B.; Brothers, S. M.; Hall, M. B.; Darensbourg, M. Y. *Dalton Trans.* **2011**, *40*, 6047−6053.

(19) Hess, J. L.; Conder, H. L.; Green, K. N.; Darensbourg, M. Y. *Inorg. Chem.* **2008**, *47*, 2056−2063.

(20) Almaraz, E.; Foley, W. S.; Denny, J. A.; Reibenspies, J. H.; Golden, M. L.; Darensbourg, M. Y. *Inorg. Chem.* **2009**, *48*, 5288−5295.

(21) Jenkins, R. M.; Pinder, T. A.; Hatley, M. L.; Reibenspies, J. H.; Darensbourg, M. Y. *Inorg. Chem.* **2011**, *50*, 1849−1855.

(22) Hansen, L.; Xu, X.; Lipowska, M.; Taylor, A.; Marzilli, L. G. *Inorg. Chem.* **1999**, *38*, 2890−2897.

(23) Rao, T. N.; Adhikesavalu, D.; Camerman, A.; Fritzberg, A. R. *J. Am. Chem. Soc.* **1990**, *112*, 5798−5804.

(24) Vanin, A. F. *Biochemistry (Moscow)* **1998**, *63*, 782−793.

(25) Vanin, A. F.; Poltorakov, A. P.; Mikoyan, V. D.; Kubrina, L. N.; Burbaev, D. S. *Nitric Oxide* **2010**, *23*, 136−149.

(26) Enemark, J. H.; Feltham, R. D. *Coord. Chem. Rev.* **1974**, *13*, 339−406.

(27) Vithayathil, A. J.; Ternberg, J. L.; Commoner, B. *Nature* **1965**, *207*, 1246−1249.

(28) Foster, M. W.; Cowan, J. A. *J. Am. Chem. Soc.* **1999**, *121*, 4093−4100.

(29) Hess, J. L.; Hsieh, C.-H.; Reibenspies, J. H.; Darensbourg, M. Y. *Inorg. Chem.* **2011**, *50*, 8541−8552.

(30) Tinberg, C. E.; Tonzetich, Z. J.; Wang, H.; Do, L. H.; Yoda, Y.; Cramer, S. P.; Lippard, S. J. *J. Am. Chem. Soc.* **2010**, *132*, 18168−18176.

(31) Hung, M.-C.; Tsai, M.-C.; Lee, G.-H.; Liaw, W.-F. *Inorg. Chem.* **2006**, *45*, 6041−6047.

(32) Tsai, M.-L.; Hsieh, C.-H.; Liaw, W.-F. *Inorg. Chem.* **2007**, *46*, 5110−5117.

(33) Wang, J.-H.; Chen, C.-H. *Inorg. Chem.* **2010**, *49*, 7644−7646.

(34) Hsieh, C.-H.; Darensbourg, M. Y. *J. Am. Chem. Soc.* **2010**, *132*, 14118−14125.

(35) Tsai, F.-T.; Chiou, S.-J.; Tsai, M.-C.; Tsai, M.-L.; Huang, H.-W.; Chiang, M.-H.; Liaw, W.-F. *Inorg. Chem.* **2005**, *44*, 5872−5881.

(36) Mills, D. K.; Reibenspies, J. H.; Darensbourg, M. Y. *Inorg. Chem.* **1990**, *29*, 4364−4366.

(37) Houser, R. P.; Tolman, W. B. *Inorg. Chem.* **1995**, *34*, 1632−1633.
(38) Kruger, H. J.; Peng, G.; Holm, R. H. *Inorg. Chem.* **1991**, *30*, 734−742.
(39) Darensbourg, D. J.; Kump, R. L. *Inorg. Chem.* **1978**, *17*, 2680−2682.
(40) Haymore, B.; Feltham, R. D.; Morris, B. E.; Clement, R. A. *Inorganic Synthesis;* John Wiley & Sons, Inc.: Hoboken, NJ, 2007; 81−89.
(41) *APEX2,* Version 2009. 7−0; Bruker AXS, Inc.: Madison, WI, 2007.
(42) *SAINTPLUS,* 1034 Version 6.63 ed.; Bruker AXS, Inc.: Madison, WI, 2007.
(43) Sheldrick, G. *SADABS;* Bruker AXS, Inc.: Madison, WI, 1999.
(44) Sheldrick, G. *SHELXS-97, SHELKL-97;* Institut fur Anorganische Chemie der Universitat Göttingen: Göttingen, Germany, 1997.
(45) Frisch, M. J.; Trucks, G. W.; Schlegel, H. B.; Scuseria, G. E.; Robb, M. A.; Cheeseman, J. R.; Scalmani, G.; Barone, V.; Mennucci, B.; Petersson, G. A.; Nakatsuji, H.; Caricato, M.; Li, X.; Hratchian, H. P.; Izmaylov, A. F.; Bloino, J.; Zheng, G.; Sonnenberg, J. L.; Hada, M.; Ehara, M.; Toyota, K.; Fukuda, R.; Hasegawa, J.; Ishida, M.; Nakajima, T.; Honda, Y.; Kitao, O.; Nakai, H.; Vreven, T.; Montgomery, J. A., Jr.; Peralta, J. E.; Ogliaro, F.; Bearpark, M.; Heyd, J. J.; Brothers, E.; Kudin, K. N.; Staroverov, V. N.; Kobayashi, R.; Normand, J.; Raghavachari, K.; Rendell, A.; Burant, J. C.; Iyengar, S. S.; Tomasi, J.; Cossi, M.; Rega, N.; Millam, J. M.; Klene, M.; Knox, J. E.; Cross, J. B.; Bakken, V.; Adamo, C.; Jaramillo, J.; Gomperts, R.; Stratmann, R. E.; Yazyev, O.; Austin, A. J.; Cammi, R.; Pomelli, C.; Ochterski, J. W.; Martin, R. L.; Morokuma, K.; Zakrzewski, V. G.; Voth, G. A.; Salvador, P.; Dannenberg, J. J.; Dapprich, S.; Daniels, A. D.; Farkas, Ö.; Foresman, J. B.; Ortiz, J. V.; Cioslowski, J.; Fox, D. J. *Gaussian 09,* Revision B.01; Gaussian, Inc.: Wallingford, CT, 2009.
(46) Becke, A. D. *Phys. Rev. A* **1988**, *38*, 3098−3100.
(47) Perdew, J. P. *Phys. Rev. B* **1986**, *33*, 8822−8824.
(48) Krishnan, R.; Binkley, J. S.; Seeger, R.; Pople, J. A. *J. Chem. Phys.* **1980**, *72*, 650−654.
(49) Wachters, A. J. H. *J. Chem. Phys.* **1970**, *52*, 1033−1036.
(50) Hay, P. J. *J. Chem. Phys.* **1977**, *66*, 4377−4384.
(51) Berger, A.; Dolg, M.; Kuechle, W.; Stoll, H.; Preuss, H. *Mol. Phys.* **1993**, *80*, 1431.
(52) Brothers, S. M.; Darensbourg, M. Y.; Hall, M. B. *Inorg. Chem.* **2011**, *50*, 8532−8540.
(53) Miertus, S.; Scrocco, E.; Tomasi. *J. Chem. Phys.* **1981**, *55*, 117.
(54) Cammi, R.; Tomasi, J. *J. Comput. Chem.* **1995**, *16*, 1449.
(55) Mennucci, B. *Wiley Interdiscip. Rev.: Comput. Mol. Sci.* **2012**, *2*, 386−404.
(56) *AMPAC 9;* Semichem, Inc.: Shawnee, KS, 1992−2008.
(57) Anderson, J.; Anderson, W.; Hieber, J.; Mitarbeitern. *Z. Anorg. Allg. Chem.* **1932**, *208*, 238−248.
(58) Denny, J. A.; Foley, W. S.; Almaraz, E.; Reibenspies, J. H.; Bhuvanesh, N.; Darensbourg, M. Y. *Dalton Trans.* **2012**, *41*, 143−148.
(59) Hess, J. L.; Hsieh, C.-H.; Brothers, S. M.; Hall, H. B.; Darensbourg, M. Y. *J. Am. Chem. Soc.* **2011**, *133*, 20426−20434.
(60) Hsieh, C.-H.; Pulukkody, R.; Darensbourg, M. Y. *Chem. Commun.* **2013**, *49*, 9326−9328.
(61) Pulukkody, R.; Kyran, S. J.; Bethel, R. D.; Hsieh, C.-H.; Hall, M. B.; Darensbourg, D. J.; Darensbourg, M. Y. *J. Am. Chem. Soc.* **2013**, *135*, 8423−8430.
(62) Bryar, T. R.; Eaton, D. R. *Can. J. Chem.* **1992**, *70*, 1917−1926.
(63) Munzarová, M. L.; Kubáček, P.; Kaupp, M. *J. Am. Chem. Soc.* **2000**, *122*, 11900−11913.
(64) Hsieh, C.-H.; Ding, S.; Erdem, O. F.; Crouthers, D. J.; Liu, T.; McCrory, C. C. L.; Lubitz, W.; Popescu, C. V.; Reibenspies, J. H.; Hall, M. B.; Darensbourg, M. Y. *Nat. Commun.* **2014**, *5*, 3684.